JACS
JOURNAL OF THE AMERICAN CHEMICAL SOCIETY
Article
pubs.acs.org/JACS

Nano-Gold Corking and Enzymatic Uncorking of Carbon Nanotube Cups

Yong Zhao,[†] Seth C. Burkert,[†] Yifan Tang,[†] Dan C. Sorescu,[‡] Alexandr A. Kapralov,[§] Galina V. Shurin,[∥] Michael R. Shurin,[∥,⊥] Valerian E. Kagan,[§] and Alexander Star*[,†]

[†]Department of Chemistry, University of Pittsburgh, Pittsburgh, Pennsylvania 15260, United States
[‡]National Energy Technology Laboratory, U.S. Department of Energy, Pittsburgh, Pennsylvania 15263, United States
[§]Department of Environmental and Occupational Health, University of Pittsburgh, Pittsburgh, Pennsylvania 15261, United States
[∥]Department of Pathology, and [⊥]Department of Immunology, University of Pittsburgh Medical Center, Pittsburgh, Pennsylvania 15261, United States

Supporting Information

ABSTRACT: Because of their unique stacked, cup-shaped, hollow compartments, nitrogen-doped carbon nanotube cups (NCNCs) have promising potential as nanoscale containers. Individual NCNCs are isolated from their stacked structure through acid oxidation and subsequent probe-tip sonication. The NCNCs are then effectively corked with gold nanoparticles (GNPs) by sodium citrate reduction with chloroauric acid, forming graphitic nanocapsules with significant surface-enhanced Raman signature. Mechanistically, the growth of the GNP corks starts from the nucleation and welding of gold seeds on the open rims of NCNCs enriched with nitrogen functionalities, as confirmed by density functional theory calculations. A potent oxidizing enzyme of neutrophils, myeloperoxidase (MPO), can effectively open the corked NCNCs through GNP detachment, with subsequent complete enzymatic degradation of the graphitic shells. This controlled opening and degradation was further carried out in vitro with human neutrophils. Furthermore, the GNP-corked NCNCs were demonstrated to function as novel drug delivery carriers, capable of effective (i) delivery of paclitaxel to tumor-associated myeloid-derived suppressor cells (MDSC), (ii) MPO-regulated release, and (iii) blockade of MDSC immunosuppressive potential.

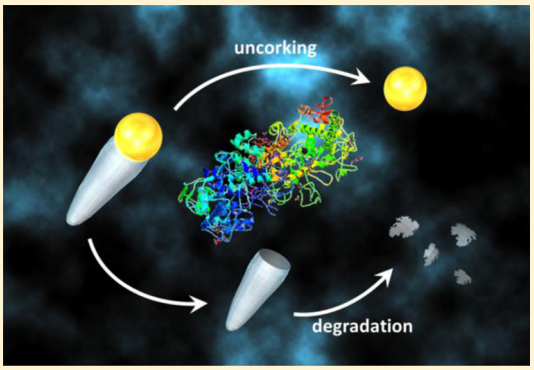

INTRODUCTION

Because of their enhanced permeability and retention effect in tumor tissues,[1] the emerging use of nanocarriers such as liposomes, nanoparticles, and macromolecules has exhibited compelling promises in drug delivery applications,[2−4] providing fundamental advantages such as longer circulation time, lower immunogenicity, better biocompatibility, and selective targeting.[5−7] In particular, given their nanoscale dimensions and versatile reactivities, carbon nanomaterials such as carbon nanotubes (CNTs) and graphene conjugates have received increasing research attention for drug delivery.[8−10] Drugs loaded on the outer surface of CNTs via covalent[9] or noncovalent[11] functionalization risk unnecessary exposure causing side-effects or early drug degradation.[12] Comparatively, filling drugs into the hollow interior of nanotubes is more desirable in terms of protecting drugs from reaction before reaching the target.[13−15] Accordingly, nitrogen-doped carbon nanotube cups (NCNCs), a cup-shaped carbon nanostructure derived from nitrogen-doped CNTs, may serve as ideal drug delivery carriers. Their small sizes ranging from 50−200 nm may exhibit a delayed rate of bloodstream clearance by the mononuclear phagocytic system (MPS),[16,17] and the unique morphology allows easy access to both their inner and outer surfaces for diverse functionalization.[18−20]

Being well recognized for their oxygen-reduction catalytic activity,[21−23] as-synthesized NCNCs consist of cup-shaped compartments stacked up via van der Waals interactions,[24] which can be readily separated into individual nanocups by various methods.[18,20,25−27] Recently, we found that a combination of preoxidation and high-intensity probe-tip sonication greatly improved the efficiency of separation, which yielded mostly individual hydrophilic nanocups.[28] Because of the intrinsic nitrogen functionalities localized at the cup opening, the separated NCNCs show strong affinity to gold nanoparticles (GNPs) in aqueous solution, which preferentially "cork" the opening of nanocups, forming self-confined nanocapsules. The hydrophilic surfaces of NCNCs after oxidation impede adsorption of opsonin proteins, which may inhibit early phagocytotic removal and ensure prolonged blood circulation for NCNCs,[29] leading to promising drug delivery applications.

Received: April 2, 2014
Published: December 21, 2014

DOI: 10.1021/ja511843w
J. Am. Chem. Soc. 2015, 137, 675−684

Despite the preferred confined morphology for drug delivery, strategies need to be sought to trigger the opening of the nanocapsules for potential release of their cargos, typically under stimuli involving chemicals, pH, or light.[30−32] On the other hand, the nanocarriers should be subject to clearance after delivery to mitigate their potential in vivo toxicity, especially for carbon nanomaterials.[33,34] Additionally, nitrogen-doped CNTs were found to be more biocompatible than undoped single- or multiwalled CNTs.[35,36] Naturally existing peroxidases, such as horseradish peroxidase (HRP) and myeloperoxidase (MPO) in combination with hydrogen peroxide (H_2O_2), can act as strong oxidation agents to enzymatically degrade carbon nanomaterials such as single- and multiwalled CNTs and graphene conjugates in vitro or in vivo.[37−41] In this work, human MPO (hMPO) was applied to degrade the GNP-corked NCNCs in the presence of H_2O_2 and NaCl, by building a stronger enzymatic oxidation system via both hMPO reactive intermediates and sodium hypochlorite (NaClO) generated by the peroxidase and halogenation cycles.[34,39] Interestingly, we found that at the initial stage of degradation, the enzyme triggered the release of GNP corks from the nanocups, which actively opened the cups, followed by a complete degradation of NCNC shells within a course of 20 days. Such triggered opening of corked nanocups was also observed in the presence of human neutrophils, a type of leukocytes capable of releasing MPO upon activation during the inflammatory response.[42] These findings may lead to an innovative drug release scheme carried out by the innate immune system, which may find potential applications for treating chronic inflammation or cancer, where antibiotics and/or protection agents can be delivered upon the enzymatic release triggered by activated immune cells.[43] To illustrate the potential of corked NCNCs as drug delivery systems, loading with a common fluorescent dye, Rhodamine 123, as well as a chemotherapeutic agent, paclitaxel (Taxol), was performed. By using Raman spectroscopy, we were able to prove the loading of the desired cargo inside corked NCNCs. Furthermore, paclitaxel loaded NCNCs were shown to effectively deliver their payload to myeloid-derived suppressor cells (MDSC), which express up-regulated amounts of MPO[44] and are responsible for the immunosuppressive response in cancer and tumor escape.[45] The delivery of paclitaxel caused inhibition of immunosuppressive phenotype of MDSC and their differentiation into dendritic cells, thus reversing their immunosuppressive activity, providing proof of concept for corked and loaded NCNCs as a novel drug delivery system.

EXPERIMENTAL SECTION

Synthesis of Separated NCNCs. The stacked NCNCs were synthesized using chemical vapor deposition (CVD) method from a liquid precursor consisting of 10.0 wt % of acetonitrile, 0.75 wt % of ferrocene, and 89.25 wt % of xylenes.[20] To perform NCNC separation, 10 mg of the as-synthesized material was dispersed into 40 mL of 3:1 (v/v) H_2SO_4/HNO_3 in a round bottle flask. The mixture was sonicated in a water bath sonicator for 4 h at room temperature, then diluted with water and washed repeatedly with 0.01 M NaOH, 0.01 M HCl, and water. The oxidized NCNCs in water were then sonicated for 8 h with a probe-tip ultrasonicator (Qsonica Q500) equipped with a 1/2 in. probe. The solution was centrifuged at 4000−8000 rpm for 15 min, and the supernatant was collected and filtered through a 200 nm-pore PTFE membrane. The filtrate containing short separated NCNCs was collected.

Corking of NCNCs with GNPs. 250 μL of $HAuCl_4$ aqueous solution (1 mg/mL) was added into 5 mL of ∼0.01 mg/mL separated NCNC aqueous solution when stirring on a hot plate at 70 °C. After 20 min of incubation, 150 μL of 1 wt % trisodium citrate solution was added dropwise, and the reaction was stirred for another 2 h. GNP/NCNC conjugates were precipitated from free GNPs by centrifugation at 3400 rpm for 15 min. For effective loading of corked NCNCs, the desired cargo was also added to the solution during corking. To load rhodamine 123 in the NCNC capsules, 5 mL of ∼0.01 mg/mL separated NCNC solution was first added with 50 μL of 15 μM rhodamine 123 in aqueous solution; for paclitaxel loading, paclitaxel was added at a final concentration of 0.25 mg/mL to the NCNC solution with the same concentration, and then the same GNP functionalization procedures were carried out. Once the loaded GNP/NCNC conjugates were collected from centrifugation, they were thoroughly suspended in 10 mL of nanopure water and centrifuged at 3400 rpm for 15 min, the supernatant was removed, and the GNP/NCNC conjugate pellet was washed four more times in the same manner.

Materials Characterization. Transmission electron microscopy (TEM) at lower resolution was performed with an FEI Morgagni microscope at an accelerating voltage of 80 kV. High-resolution TEM was performed on a JEOL 2100F microscope with 200 kV accelerating voltage. Samples were drop-casted on a lacey carbon TEM grid. The cell samples were first subjected to a protease k digest. Raman spectra were taken on a Renishaw inVia Raman microscope with an excitation wavelength of 633 nm at 50% laser intensity and 10 s exposure time unless noted otherwise. X-ray photoelectron spectroscopy (XPS) was performed on a Thermo Scientific K-Alpha using monochromated Al Kα X-rays as the source. UV−vis spectroscopy was carried out on a PerkinElmer Lambda 900 spectrometer. Energy-dispersive X-ray (EDX) spectroscopy was performed on a Phillips XL30 FEG microscope equipped with an EDAX assembly. Dynamic light scattering (DLS) was performed using a quasi-elastic light scattering spectrometer (Brookhaven 90 Plus Particle Size Analyzer).

Enzyme-Triggered Opening and Degradation of GNP-Corked NCNCs. The separated NCNCs with or without GNPs were dispersed at a concentration of 0.015 mg/mL into 0.01 M phosphate buffer solution in a total volume of 1000 μL. The enzymatic degradation was conducted following published procedure.[39] To the NCNC sample, NaCl at a concentration of 1 μM is added on the initial day; lyophilized purified native human MPO (Athens Research and Technology, Inc.) is added daily at a concentration of 8.35 μg/mL; 1 μL of 100 mM H_2O_2 is added every 2 h, four times per day. For the NaClO degradation experiment, 1 μL of 100 mM NaClO was added every 2 h, four times per day in the absence of hMPO and H_2O_2. For the H_2O_2 control experiment, 1 μL of 100 mM H_2O_2 was added every 2 h, four times per day in the absence of hMPO, NaCl, and NaClO. The hMPO/H_2O_2 control was the same as the active sample but without NaCl. All samples were incubated at 37 °C for 20 days, with daily agitation by vortex shaker for better dispersion.

Neutrophils Isolation and Incubation with Nanocups. Human neutrophils were isolated by a procedure utilizing Histopaque (Sigma, St. Louis, MO). Briefly, human buffy coat (Central Blood Bank, Greentree, PA) was mixed with 6% Dextran T-500 in phosphate-buffered saline (PBS) in a 5:1 ratio and allowed to sediment for 30 min at room temperature. The leukocyte-rich plasma (top layer) was aspirated, diluted two times with PBS, layered over Histopaque solution with a density of 1.077 g/mL (Sigma, St. Louis, MO), and subjected to centrifugation (700g for 45 min at room temperature without brake). The pellet containing neutrophils was collected, and contaminated erythrocytes were removed by brief hypotonic lysis with ice-cold water. Neutrophils were washed twice with calcium and magnesium free PBS, and suspended in RPMI-1640 without phenol red, containing 10% fetal bovine serum with a concentration of 10×10^6 cells/mL. 50 μg of nanocups incubated with purified human IgG (Invitrogen, Carlsbad, CA) in a 1:1 ratio (w/w) for 18 h at 37 °C were incubated with neutrophils (25×10^6) for 16 h, and the extent of biodegradation was assessed.

hMPO Contents in Cells and Its Release. Levels of hMPO in cells were determined by an ELISA kit (Alpco Diagnostics, NH) after 30 min incubation with samples. Neutrophils were centrifuged at

DOI: 10.1021/ja511843w
J. Am. Chem. Soc. 2015, 137, 675−684

1000*g* for 10 min. The supernatant and pellet were obtained and used separately for hMPO measurements according to the manufacturer's manual. The amounts of hMPO were expressed as mg/mL.

Animals. Pathogen-free C57BL/6 mice (7−8 wk old) from Jackson Laboratories (Bar Harbor, ME) were individually housed and acclimated for 2 weeks. Animals were supplied with water and food ad libitum and housed under controlled light, temperature, and humidity conditions. All animal studies were conducted under a protocol approved by the Institutional Animal Care and Use Committee.

Tumor Cells and Experimental Procedures. B16 melanoma cells were obtained from American Type Culture Collection (ATCC, Manassas, VA) and maintained in RPMI 1640 medium supplemented with 2 mM L-glutamine, 100 U/mL penicillin, 100 μg/mL streptomycin, 10 mM HEPES, 10% heat-inactivated FBS, 0.1 mM nonessential amino acids, and 1 mM sodium pyruvate (Invitrogen Life Technologies, Inc., Grand Island, NY). Tumor conditioned medium was collected from subconfluent cultures, centrifuged (300*g*, 15 min), and cell-free supernatant was collected, aliquoted, and used to treat MDSC.

Mice were inoculated with 1×10^5 B16 cells (300 μL PBS) via the tail vein. Twenty-one days later, the animals were sacrificed, and bone marrow and lungs were isolated.

Isolation, Treatment, and Evaluation of MDSC. For pulmonary MDSC isolation and analysis, mouse lungs were dispersed using 2% collagenase A and 0.75% DNase I (Roche Diagnostics GmbH, Mannheim, Germany) in RPMI 1640 medium supplemented with 10% FBS at 20 °C for 1 h in Miltenyi Biotec gentleMACS Dissociator. Bone marrow cells were isolated, filtered through a 70 μm cell strainer, and red blood cells were lysed with lysing buffer (155 mM NH_4Cl in 10 mM Tris-HCl buffer pH 7.5, 25 °C) for 3 min. After RBC lysis, cells were washed and used for MDSC sorting. CD11b+ Gr-1+ MDSC were isolated from the digested lungs and bone marrow cell suspensions by magnetic cell sorting using a mouse MDSC Isolation Kit (MACS, Miltenyi Biotec, Auburn, CA) according to the manufacturer's instructions. Control MDSC were isolated from tumor-free mice. After isolation, all MDSC were cultured with empty and paclitaxel-loaded corked NCNC for 48 h.

For testing the effect of NCNC on MDSC function, bone marrow-derived MDSC from tumor-free and B16-bearing mice were treated with NCNC as above and mixed with T cells at different ratios (1/10−1/100) for 24 h. Syngeneic T lymphocytes were isolated from the spleen of tumor-free mice by nylon wool enrichment method and preactivated with Concanovalin A (5 h, 2.5 μg/mL, Sigma, St. Louis, MO). T cell proliferation was measured by uptake of 3H-thymidine (1 μCi/well, 5 Ci/mmol; DuPont-NEN, Boston, MA) pulsed for 16−18 h. Cells were harvested on GF/C glass fiber filters (Whatman Intl. Ltd., Maidstone, UK) using MACH III microwell harvester (Tomtec, Hamden, CT). 3H-thymidine incorporation was determined on MicroBeta TRILUX liquid scintillation counter (WALLAC, Finland) and expressed as count per minute (cpm).

Production of TGF-β by the bone marrow MDSC isolated from tumor-free and B16-bearing mice was determined by assessing the levels of TGF-β1 in cell-free supernatants by ELISA (R&D Systems, Minneapolis, MN).

Differentiation of MDSC into DC was evaluated in lung MDSC cultures treated with NCNC for 48 h by staining cells with anti-CD11b, anti-Ly6G, anti-Ly6C, anti-Gr-1, and anti-CD11c antibodies (Biolegend Inc., San Diego, CA) directly conjugated to FITC, PE, PE/Cy7, or APC/Cy7, and analyzed by flow cytometry (BD FacsCalibur) and FlowJo software.

Statistical Analysis. Results were analyzed using one-way ANOVA and Student unpaired *t* test with Welch's correction for unequal variances. All experiments were repeated at least twice, and the results are presented as the means ± SEM (standard error of the mean). *P* values of <0.05 were considered to be statistically significant.

RESULTS AND DISCUSSION

The stacked NCNCs were synthesized following a modified chemical vapor deposition (CVD) method from a mixture of acetonitrile, ferrocene, and xylenes,[20] which were then effectively separated through acid oxidation and subsequent probe-tip sonication.[28] The separated NCNCs consist of mostly individual and short stacks of nanocups between 80−200 nm in length as revealed by transmission electron microscopy (TEM) imaging (Figure 1a) and dynamic light scattering (DLS) measurements (Supporting Information Table S1). A typical individual NCNC has a cup-shaped morphology with an opening interior of about 30 nm in diameter. The oxidation and sonication left the separated NCNCs with higher levels of graphitic defects as reflected by Raman spectroscopy (Supporting Information Figure S1), which lead to their hydrophilic nature.

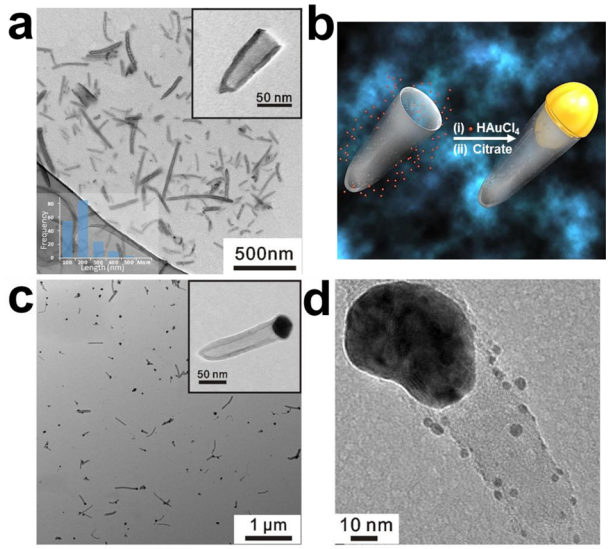

Figure 1. (a) Transmission electron microscopy (TEM) images of separated nitrogen-doped carbon nanotube cups (NCNCs). The upper right inset shows a magnified TEM image of an individual nanocup, and the lower left inset shows the length distribution of the separated cups. (b) Schematic illustration of corking NCNCs by (i) incubation with $HAuCl_4$ and (ii) sodium citrate reduction. (c) Separated NCNCs functionalized with GNP corks by sodium citrate reduction. The inset shows the TEM image of an individual nanocup corked by a GNP on the opening. Some unbound GNPs are not completely removed upon single centrifugation. (d) High-resolution TEM image of the corked GNP/NCNC structure.

The intrinsic nitrogen functionalities are preferentially located at the open rim of the separated nanocups, preventing them from further growth during CVD synthesis[46] and providing reactive sites on the open rims of the separated NCNCs.[20] The separated NCNCs form a stable water dispersion for months, allowing the growth of GNPs directly on the nanocups by sodium citrate reduction. Briefly, chloroauric acid was first mixed with NCNCs aqueous suspension for 20 min, and sodium citrate was then added to the reaction mixture at 70 °C (Figure 1b). Upon removal of free GNPs by centrifugation, elemental analysis from energy-dispersive X-ray (EDX) spectroscopy confirmed the existence of Au on NCNCs (Supporting Information Table S2). TEM images show that almost every nanocup was evenly decorated with 1−2 GNPs of about 30 nm in diameter. A large proportion

DOI: 10.1021/ja511843w
J. Am. Chem. Soc. 2015, 137, 675−684

up to 37% of the NCNCs have their open rims bound with GNPs (Supporting Information, Efficiency of GNP Corking), which effectively form stoppers corking the nanocups (Figure 1c). Once bound to the rim of the cups, the GNPs appear to adapt the shape of the opening seamlessly and completely seal their interior space, as shown by high-resolution TEM image (Figure 1d). High-resolution TEM images magnified from Figure 1d reveal the polycrystalline nature of the GNP cork with lattice distance of 0.23 nm corresponding to gold (111) surfaces, which suggest that the GNP corks are the result of welding many fcc gold nanocrystals (Supporting Information Figure S2a).[47,48] Small gold nanocrystals were also found sparsely bound on the graphitic sidewalls of the nanocups (Supporting Information Figure S2b), suggesting that the cup opening is the more favored site for GNP growth.

The UV−vis absorption spectra of separated NCNCs show a characteristic peak located at 260 nm (Figure 2a), corresponding to the π electron plasmon band in conjugated systems.[49] After GNP growth, the reaction mixture turned from brown to red, and the NCNC/GNP conjugates were collected by centrifugation. There is a distinct color difference between the red supernatant and the purple precipitate suspensions, which is confirmed by the red-shift of the gold surface plasmon resonance (SPR) band from 526 to 538 nm (Figure 2a). This red-shift may be due to both the size difference (Supporting Information Figure S3) and the direct electronic interaction between the GNPs and the NCNC substrate.[20] The presence of GNPs on NCNCs causes a strong surface-enhanced Raman scattering (SERS) effect, allowing sensitive detection of this hybrid material by Raman spectroscopy in biological samples. Figure 2b shows the Raman spectra of NCNCs decorated with GNPs as compared to unfunctionalized NCNCs. Enhancements of about 15- and 18-fold were noticed for the intensities of D (~1350 cm^{-1}) and G (~1582 cm^{-1}) bands, respectively. We speculate that the SERS effect mainly originated from the charge transfer between GNPs and NCNCs[50] due to the electronic interaction between GNPs and NCNCs, as a result of direct contact. By physically mixing NCNCs with commercial citrate-coated GNPs, free GNPs are randomly distributed together with NCNCs showing no specific interaction (Supporting Information Figure S4); the SERS effect was not observed (Figure 2b). On the other hand, the functionalization of GNPs is more favorable on the nitrogen-doped graphitic structure. Undoped multiwalled CNTs (MWCNTs) treated by the same oxidation/tip-sonication procedure did not bind effectively to GNPs, indicating that the oxygen groups are not strong anchoring sites for GNP growth (Supporting Information Figures S5, S6a).

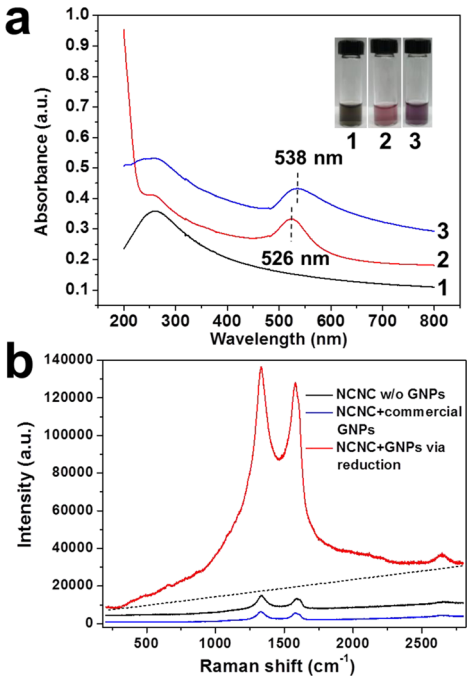

Figure 2. (a) UV−vis absorption spectra and photograph of aqueous suspensions of separated NCNCs (1), supernatant (2), and precipitate (3) of NCNC/GNP conjugates after centrifugation. (b) Raman spectra of separated NCNCs (black), NCNCs mixed with commercial GNPs (blue), and NCNCs corked with GNPs by in situ reduction process (red). The dotted line indicates the baseline.

Growth Mechanism of GNP Corks on NCNCs. Previously, we demonstrated the preferential distribution of nitrogen functionalities on the open rims of NCNCs,[20] as a result of energetic incompatibility of nitrogen in the graphitic network.[46] To understand the mechanism of the GNP cork formation, the chemical structure of nitrogen present in separated NCNCs was characterized by X-ray photoelectron spectroscopy (XPS). The nitrogen content is detected at about 2.0 and 1.4 atomic % before and after the separation process, respectively (Supporting Information Figure S6b). Different nitrogen functionalities were deconvoluted from the high-resolution N 1s profile, listed in Supporting Information Table S3. The N 1s profile of as-synthesized stacked NCNCs shows four peaks representing pyridinic, pyrrolic, graphitic, and oxidized nitrogen functionalities (Supporting Information Figure S7a). Comparatively, the separated NCNCs display a new peak at 399.8 eV (Supporting Information Figure S8), which is assigned to amine groups as proven by the Kaiser test (Supporting Information Figure S7b).[20] Before GNP functionalization, the amine groups were largely protonated ($-NH_3^+$) with a peak at 402.1 eV,[51,52] possibly as a result of acid treatment. After the sodium citrate reduction and GNP formation, most of the amine groups were deprotonated, along with the disappearance of the 402.1 eV peak and increase of the amine peak. The change of the amine groups alludes to the initial binding sites of GNPs on NCNCs. We speculate that the growth of the GNP corks begins with a nucleation step on the open rims enriched with amine groups, followed by subsequent growth under citrate reduction. Presumably, during the initial incubation, the gold precursor $AuCl_4^-$ was first electrostatically bound to the $-NH_3^+$ groups, and then reduced by the graphitic network, leading to further oxidation of carbon (Supporting Information Figure S8) and deprotonation of amines.

The growth process of the GNP corks was examined by TEM of the reaction mixture sampled at different reaction times (Figure 3a−d). The initial gold nucleation on the open rim and the subsequent welding of adjacent GNP seeds are observed during the first 20 min of reaction. After addition of sodium citrate to the reaction mixture, the formation of GNPs was further accelerated. After 50 min, the agglomeration of GNP seeds on the opening of nanocups has occupied the entire rim, which eventually leads to the formation of molded GNP corks after 80 min of reaction. The corresponding UV spectra during the reaction show the appearance of the gold SPR band after 50 min, with a gradual red-shift indicating the increasing size of GNPs (Supporting Information Figure S9).

DOI: 10.1021/ja511843w
J. Am. Chem. Soc. 2015, 137, 675−684

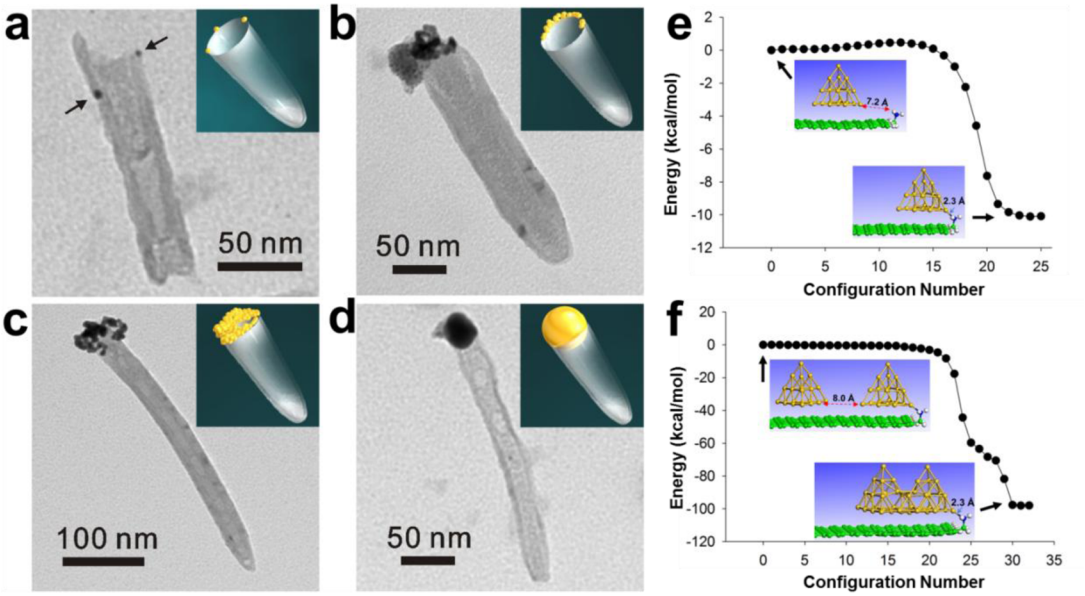

Figure 3. TEM images of the growth process of GNPs on individual NCNCs sampled at (a) 5 min, (b) 20 min, (c) 50 min, and (d) 80 min after the addition of $HAuCl_4$. Sodium citrate was added at 20 min right after the sampling. The arrows in (a) show the nucleation of gold seeds. Minimum energy reaction pathways for diffusion of Au_{20} cluster from the central region of the (7 × 11) graphene flake surface toward the zigzag edge (e) decorated with a CH_2NH_2 group and (f) when a second Au_{20} cluster is anchored to the $-CH_2NH_2$ group at the graphene edge. For both sets of pathways, the initial and final configurations are represented in the inset panels. Legend of atoms: C, green; N, blue; H, white; O, red; and Au, orange.

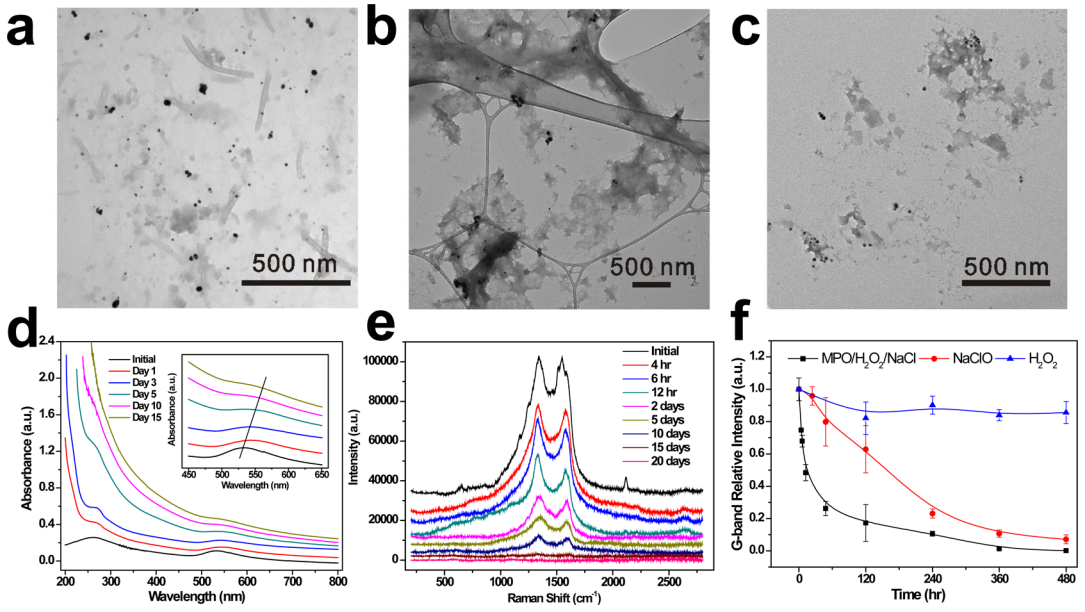

Figure 4. TEM images of the degradation process of NCNCs functionalized with GNPs under hMPO/H_2O_2/NaCl at (a) day 5, (b) day 10, and (c) day 20. (d) UV−vis spectra and (e) Raman spectra of the sample during degradation. The inset in (d) shows the red-shift of the GNP SPR band. (f) Intensity plots of the Raman G bands from the active sample (black), the NaCl control (red), and the H_2O_2 control (blue). The intensity was averaged and normalized to the initial value, and the error bars correspond to the standard errors of the mean.

The observed nucleation of GNP seeds on the NCNC openings and subsequent growth into GNP corks was further supported by first-principles calculations (Supporting Information, Computational Methods). We simulated the initial stage of the nucleation process for the case of a Au_{20} cluster adsorbed initially either at the center or at the edge of a 7 × 11 graphene flake functionalized with different nitrogen functional groups (Supporting Information Figure S10). By comparing the adsorption energy at the most stable binding configurations, we found that the graphene edge functionalized with an aliphatic primary amine ($-CH_2NH_2$) incurred the strongest binding with Au_{20}. In this case, the $-CH_2NH_2$ group is extruding out of the graphene plane such that the lone electron pair from N is unconjugated and forms a covalent bond with the Au_{20} cluster (Figure 3e). The existence of primary amine groups on separated NCNCs is confirmed by XPS, and quantified by the Kaiser test to be approximately 5 μmol per gram of NCNCs (Supporting Information, Figures S7, S8);[20,28]

DOI: 10.1021/ja511843w
J. Am. Chem. Soc. 2015, 137, 675−684

therefore, the anchoring effect of amine groups explains the nucleation mechanism during GNP growth. The energy plot in Figure 3e shows the minimum energy reaction pathway of the Au_{20} cluster migrating from the central region of the graphene flake toward the edge where it bonds with a $-CH_2NH_2$ group. The reaction profile demonstrates that anchoring of the Au_{20} cluster mediated by this group is highly favorable and the diffusion barriers involved are very small (<0.5 kcal/mol). In addition, when a given Au_{20} cluster is already bound to the $-CH_2NH_2$ group, another Au cluster can easily diffuse toward it and bind forming a larger cluster through a nanowelding process (Figure 3f).[47] This cumulative effect eventually leads to formation of large GNPs preferentially on the opening of the NCNCs, where the graphitic edges are enriched with amine groups.

Enzyme-Triggered Uncorking and Degradation of GNP/NCNCs. While the confinement of the interior of NCNCs with GNP corks endows the nanocups with potential as drug delivery carriers, the enzymatic degradation ensures the subsequent optimized release of the payloads and clearance of the nanocup shells for improved biocompatibility. The stacked nitrogen-doped CNTs were previously shown to undergo a slow degradation by plant HRP/H_2O_2 initiated at the defect sites on graphitic surface over the period of 90 days.[40] Using a biomedically more relevant oxidative enzyme hMPO, we hereby examined the degradation of separated NCNCs. The separated NCNCs were dispersed in phosphate buffer solution containing 1 mM NaCl, which is necessary for producing NaClO in the halogenation cycle. With daily supplements of MPO and H_2O_2, the separated NCNCs were seen gradually degraded within 20 days, as evidenced by the morphological deformation from TEM images, and the suppression of their UV−vis and Raman characteristic peaks (Supporting Information Figure S11). On the other hand, with only NaClO as oxidant, incomplete degradation was observed during the 20-day time frame (Supporting Information Figure S12), which indicates that the synergetic effect of the peroxidase and halogenation cycles is important to expedite the degradation of NCNCs.[39] As the control, without hMPO or NaClO as oxidants, only H_2O_2 did not incur any significant degradation of NCNCs (Supporting Information Figure S13).

Interestingly, when the NCNCs were corked with GNPs, we found that the hMPO not only degraded the graphitic shell, but also triggered the opening of nanocups by releasing the GNP corks at the early stage of incubation. The initial GNP/NCNC sample was centrifuged several times to ensure the removal of free GNPs. With daily additions of hMPO and H_2O_2 to the sample in the presence of NaCl, TEM images show that most of the GNPs were detached from NCNCs within the first 5 days of degradation (Figure 4a). Subsequently, the NCNCs underwent significant degradation after releasing the GNP corks and eventually vanished after 20 days (Figure 4b,c), leaving only agglomerations of GNPs. UV−vis spectra in Figure 4d show the similar trend of disappearing π electron band within 15 days of degradation. Notably, the SPR band from GNPs was observed to gradually red-shift from an initial of 538 to 561 nm. We infer that this red-shift is due to the agglomeration of free GNPs detached from NCNCs, because the GNP corks are not entirely coated with citrate leaving bare active surfaces that can easily weld with each other.[47] Once detached, the GNPs failed to induce the surface-enhanced Raman effect on NCNCs. The Raman spectra of the degradation sample show a drastic decrease of D and G band intensities within the first 2 days of degradation, followed by a slower decrease afterward until a complete suppression (Figure 4e). After the GNPs are detached, the D to G band ratio returns to normal, in which the D band is much higher than the G band (Supporting Information Figure S1). However, when the degradation was carried out in the NaClO-only sample, the GNP corks largely remained attached on the nanocups without apparent agglomeration, until most nanocups were degraded (Supporting Information Figure S14). The attachment of GNPs on the NCNCs was evidenced by the absence of red-shift in their SPR bands, as well as a strong lasting SERS effect within the first 5 days of degradation. When the GNP/NCNCs were incubated with only H_2O_2, no significant detachment of GNPs or degradation of NCNCs was observed (Supporting Information Figure S15).

The different behaviors of the GNP/NCNC conjugates under different degradation conditions were monitored by the intensity plot of the G band from Raman spectra (Figure 4f). Each data point was averaged from five Raman spectra at different spots and normalized to the initial intensity. Two decreasing stages are distinguished in the hMPO/H_2O_2/NaCl sample: The fast-decaying stage during the first 2 days corresponding to the detachment of GNPs from NCNCs when they mostly aggregated and lost direct interaction with NCNCs. The second stage reflects the actual degradation of nanocups, which shows a slower but complete decay within 20 days. In contrast, the intensity plot in the NaClO sample shows a slower and more constant decreasing slope throughout the 20 days, largely due to the loss of graphitic structure instead of GNP detachment. The plot in the H_2O_2 control remains stable during the experiment, indicating that the GNP/NCNC conjugate is stable under physiological conditions. The Raman plots confirm that the interaction with hMPO uniquely triggers the dissociation of GNPs from NCNCs, which is not due to simple oxidation of the graphitic shell. We speculate that the detachment of GNPs is caused by the strong binding of hMPO toward the defective sites of NCNCs during the peroxidase cycle and the interaction with negatively charged GNPs,[39] with corresponding weakening of the interaction between GNPs and nanocups. On the other hand, the ClO^- produced in the halogenation cycle is a strong oxidant that oxidizes the whole graphitic framework with no preferential binding sites[53] and has a limited effect on GNPs. To prove the uncorking effect from the peroxidase cycle, we incubated the GNP/NCNCs in the presence of hMPO and H_2O_2 in the absence of NaCl. It turned out that the GNPs were readily detached from NCNCs during the first 5 days, inducing a red-shift of the SPR band and a sudden drop of Raman intensity, while the NCNCs were not significantly degraded throughout the 20 days (Supporting Information Figure S16).

The hMPO-triggered uncorking and degradation of GNP/NCNCs was further studied in vitro with human neutrophils, a type of immune cells primarily involved in inflammatory responses and MPO generation.[34] Using ELISA kit, we found that neutrophils contained 1.8 mg hMPO per 10^6 neutrophils. Upon neutrophil activation, 75% of the total hMPO remained inside the cells, and only 25% of the amount of enzyme was released into the extracellular environment. The neutrophils were administered with 50 μg of GNP-corked NCNCs opsonized with IgG. After 18 h of incubation at 37 °C, the cells were then solubilized with sodium dodecyl sulfate (SDS) for analysis. TEM imaging shows that most GNPs were detached from NCNCs and aggregated with each other (Figure

DOI: 10.1021/ja511843w
J. Am. Chem. Soc. 2015, 137, 675−684

5a). Hints of degradation were observed on NCNCs as the graphitic surfaces started to deform. Comparatively, when the GNP-NCNCs were mixed with neutrophils, which were directly collected without incubation, no signs of either GNP detachment or NCNC degradation were shown (Supporting Information Figure S17a). Among ~100 NCNCs observed from different TEM images, the percentage of NCNCs decorated with GNPs is significantly reduced after the 18 h incubation (Figure 5b), suggesting that human neutrophils can effectively uncork the cups in vitro. Raman spectra (Supporting Information Figure S17b) and the Raman intensity mapping (Figure 5c,d) on the G-bands further confirmed the detachment of GNPs. The cell residues without incubation show strong signals of the nanocups due to the enhancement from the GNPs, appearing as bright yellow spots in the optical image (Figure 5c), while in the sample after the 18 h incubation, the signals from nanocups are greatly suppressed. These data indicate that the reactive MPO intermediates generated by neutrophils during the cellular inflammatory response may trigger the release of drug cargo in the potential nanocup drug delivery system.

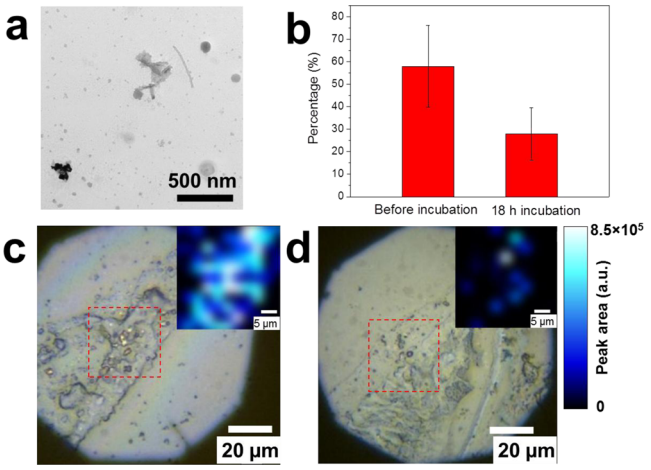

Figure 5. (a) TEM image of the GNP/NCNC sample treated with neutrophils after 18 h of incubation. (b) Ratios of the NCNCs still corked with GNPs versus total NCNCs after the neutrophil treatment, with or without 18 h of incubation. The error bars correspond to the standard errors of the mean. (c,d) Optical image of the cell tissues from the GNP/NCNC sample treated with neutrophils: (c) before and (d) after 18 h of incubation, under Raman microscope. The insets show the Raman intensity mapping of G-band corresponding to the areas inside the dashed boxes.

Loading of Drug Molecules in Corked NCNCs. With the controllable confinement and release of the cargo, the corked NCNCs exhibit potential as drug delivery vehicles. Here, we managed to load two different model drug molecules, Rhodamine 123 (Rh123) and paclitaxel, into the separated nanocups while sealing them with GNP corks. Rhodamine derivatives have been frequently used as Raman probes for high-sensitivity SERS analysis;[54] Rh123 was first mixed at the concentration of 0.15 μM with NCNCs in water, followed by incubation with chloroauric acid and reduction by sodium citrate. The solution is then repetitively washed with ethanol and water to remove any free Rh123, and TEM images showed that the presence of low concentration Rh123 did not influence the formation of GNP corks on the nanocups (Supporting Information Figure S18). For the control, Rh123 was added at the concentration of 0.15 μM to the already GNP-corked NCNC solution and also repetitively washed. To verify the encapsulation of Rh123, we took Raman spectra on both of the repeatedly washed samples. The pure Rh123 sample on a glass slide gave multiple peaks between 300 and 1700 cm^{-1} (Figure 6a), in good agreement with the literature.[55] 20 μL of active and control samples were drop-casted and dried on a glass slide, and Raman spectra were taken at a lower (10%) laser intensity to suppress the intensity from D and G bands. Before centrifugation, SERS signals of Rh123 can be detected on both the sample and the control (Supporting Information Figure S19). After repeated centrifugal wash, the active sample still shows a fairly high surface-enhanced spectrum of Rh123, but the control did not show any Rh123 signals other than the D and G bands. It is inferred that the repeated wash is able to remove any untrapped free Rh123 molecules outside the cups, while the remaining Raman signals in the active sample after wash may be incurred from the trapped Rh123 adsorbed on the inner surface of the GNP corks. In comparison, GNPs reduced by sodium citrate in the presence of Rh123 but the absence of

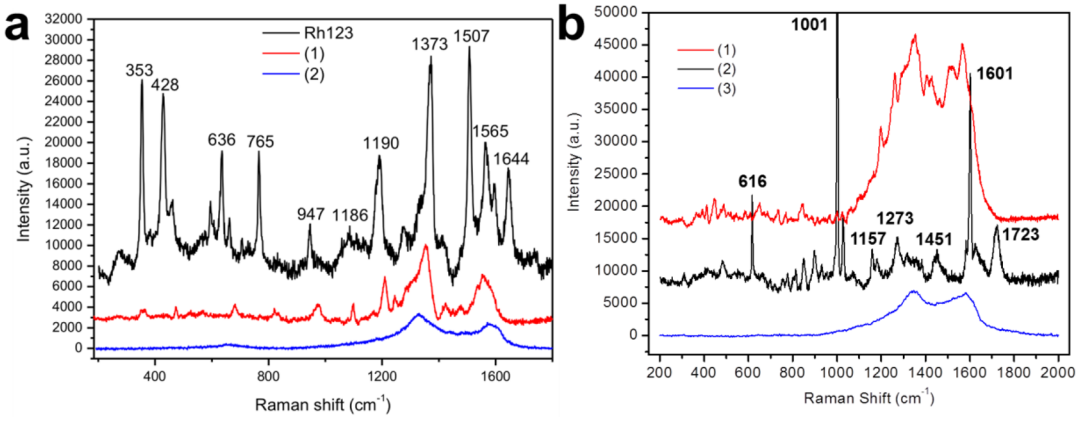

Figure 6. (a) Raman spectra of free Rh123 drop-casted on a glass slide at the concentration of 15 μM (black), (1) the precipitate of NCNCs functionalized with GNPs in the presence of 0.15 μM Rh123, after repetitive wash, and (2) the precipitate of 0.15 μM Rh123 mixed with as-functionalized NCNC/GNP conjugates, after repetitive wash; the spectrum was taken at 10% laser intensity to weaken the NCNC background. (b) (1) The surface-enhanced Raman spectroscopy of GNP-corked NCNCs loaded with paclitaxel, (2) Raman spectrum of pure paclitaxel, scaled up by 5-fold, and (3) the control, in which GNP-corked NCNCs are added with paclitaxel, after repetitive centrifugal wash.

DOI: 10.1021/ja511843w
J. Am. Chem. Soc. 2015, 137, 675−684

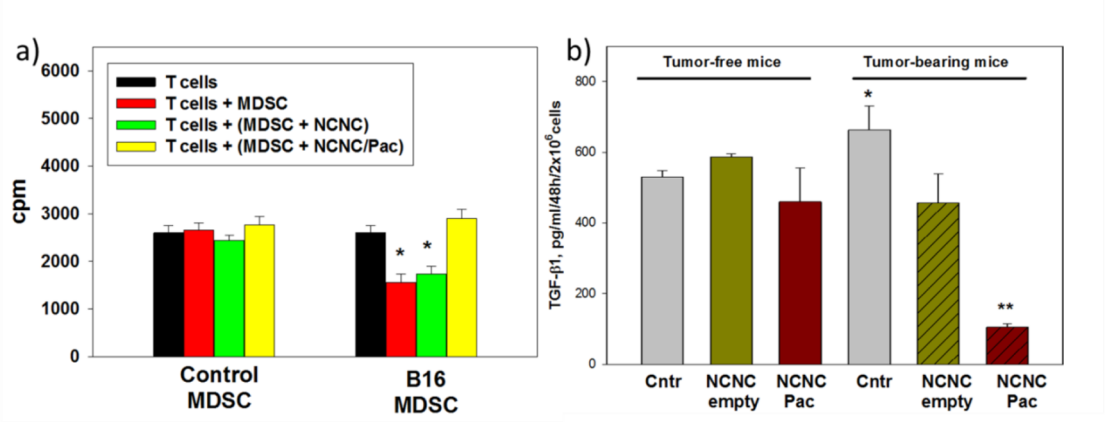

Figure 7. NCNC-delivered paclitaxel blocks immunosuppressive activity of tumor-associated MDSC. (a) Control and tumor-associated MDSC were incubated with empty and paclitaxel-loaded NCNC for 48 h, washed, counted, and coincubated with ConA preactivated and syngeneic splenic T lymphocytes. T cell proliferation was assessed by 3H-thymidine incorporation and expressed as count per minute (cpm) (*, $p < 0.05$, ANOVA). (b) Bone marrow MDSC were sorted from tumor-free mice and mice bearing B16 melanoma for 3 weeks, incubated with medium (control), empty NCNC, and NCNC/Pac. TGF-β was measured by ELISA in cell-free supernatants (*, $p < 0.05$ vs Cntr in tumor-free mice; **, $p < 0.05$ vs all groups).

NCNCs only showed very weak Raman signals of Rh123 after repetitive wash (Supporting Information Figure S19). These results suggest that Rh123 can indeed be trapped inside the nanocups after the corking of GNPs, but it is not able to bind tightly on the outer GNP surfaces. To verify the encapsulation of Rh123, fluorescence spectra of Rh123 from the sample and the control are also compared (Supporting Information Figure S20). Similarly, we loaded paclitaxel, a well-known cancer chemotherapeutic drug, into the corked NCNCs. After repetitive wash, the SER spectrum shows additional peaks within 200−1600 cm^{-1} for the paclitaxel encapsulated in the corked NCNCs (Figure 6b), matching well with the Raman spectrum of pure paclitaxel.[56] Comparatively, the GNP-corked NCNCs mixed with paclitaxel and repetitively washed showed no paclitaxel peaks, indicating no exterior adsorption of paclitaxel to the surface of corked NCNCs (Figure 6b). The slight shift of the characteristic peaks of Rh123 or paclitaxel in the corked NCNC samples from the pure chemicals can be due to band stiffening as a result of charge transfer between the GNPs and the analytes.[50] Because different vibrational modes may be enhanced differently, the relative intensities of the peaks also vary from the spectra of the pure chemical.

Targeting of MDSC by Releasing Paclitaxel. To test how corked NCNCs deliver incorporated molecules to targeted cells, we have selected tumor-associated myeloid-derived suppressor cells (MDSC), known to be involved in tumor immunosuppressive activity,[57−61] and paclitaxel (Taxol), known to block such behavior in MDSC when used in low doses.[62−66] NCNCs were corked with GNPs through sodium citrate reduction in the presence of paclitaxel to create sealed and loaded nanocarriers for delivery to MDSC as proven by Raman spectroscopy (Figure 6b). MDSC were isolated from tumor-free and melanoma-bearing mice and incubated with empty corked NCNCs and paclitaxel loaded NCNCs to determine the effect of the delivery of paclitaxel on the biological function of MDSC.

First, we proved that NCNC-delivered paclitaxel was not cytotoxic for cells by assessing MDSC apoptosis after coincubation with NCNCs. Supporting Information Figure S21 shows that no significant differences in the percentage of apoptotic (Annexin V+/PI-) cells were detected between control and tumor-associated MDSC treated with empty or paclitaxel-loaded NCNCs ($p > 0.5$). Tumor-associated MDSC are characterized by an upregulation of MPO, providing a mechanism for degradation of NCNCs and resulting delivery of loaded payload. Upon 48 h of incubation, NCNCs are readily uncorked as shown by TEM images and the decreased Raman intensity (Supporting Information Figure S22). Next, we revealed that NCNCs loaded with paclitaxel, but not empty NCNCs, blocked the ability of tumor-associated MDSC to suppress proliferation of preactivated T lymphocytes (Figure 7a) ($p < 0.05$), which suggests that paclitaxel was effectively delivered to MDSC by NCNCs and affected their immunosuppressive activity, as expected. Furthermore, knowing that TGF-β produced by tumor-associated MDSC plays a role in inhibiting T cells, we showed that NCNC/Pac, but not empty NCNCs, significantly down-regulated expression of TGF-β in tumor-associated MDSC (Figure 7b) ($p < 0.05$). As expected, no effects of empty NCNCs on control MDSC were observed (Figure 7). Finally, we have tested whether paclitaxel delivered by corked NCNCs can stimulate differentiation of tumor-associated MDSC into dendritic cells (DC), because this property of MDSC has been reported to be lost in cancer. As shown in Supporting Information Figure S23, treatment of MDSC isolated from tumor-bearing mice with NCNC/Pac, but not empty corked NCNC, increased appearance of CD11c+ DC up to 3-fold, suggesting that NCNC-delivered paclitaxel up-regulates MDSC differentiation to DC. Altogether, these results demonstrate that paclitaxel can be loaded into NCNCs, stored within the corked NCNCs, and effectively delivered to targeted cells, such as MDSC, suggesting the promising potential of GNP-corked NCNCs in novel drug delivery systems.

■ CONCLUSIONS

We developed a novel cup-shaped graphitic structure using nitrogen-doped carbon nanotube cups (NCNCs), which can be efficiently isolated from stacked nitrogen-doped CNT fibers through a combination of acid oxidation and high-intensity ultrasonication. Through a sodium citrate reduction, the separated nanocups can be effectively corked with GNPs on their open rims due to the preferential distribution of nitrogen

DOI: 10.1021/ja511843w
J. Am. Chem. Soc. 2015, 137, 675−684

functionalities on the edge. A pronounced SERS effect on these GNP-corked NCNCs was observed, indicating direct electronic interaction between GNPs and NCNCs. On the basis of both experimental and theoretical analysis, we identified the growth mechanism of the GNP corks, initiated by the nucleation of small GNP seeds toward the nitrogen functionalities, especially aliphatic amines on the opening of the cups. In addition, we demonstrated that the GNP-corked NCNCs can be effectively "opened" by hMPO, followed by a complete degradation of the graphitic cup shells. The uncorking effect was further observed in the presence of MPO-containing human neutrophils. Finally, we showed the drug loading capacity of corked NCNCs for cargo molecules such as Rh123 and paclitaxel, and found that the loaded paclitaxel can be effectively delivered to tumor-associated MDSC, inhibiting their immunosuppressive activity. The findings indicate the potential of the GNP-corked NCNCs in drug delivery applications, particularly as a novel immunotherapy for chronic inflammation, or cancer treatments.

■ ASSOCIATED CONTENT

Supporting Information

Computational methods, average lengths, elemental composition, Raman spectra, additional TEM and high-resolution TEM images, control experiment of NCNCs mixed with commercial GNPs, control experiment of nondoped MWCNTs, survey XPS of MWCNTs and NCNCs, N 1s XPS of NCNCs and UV−vis of Kaiser test, N 1s and C 1s XPS of NCNCs before and after corking, UV−vis spectra of NCNCs at different GNP corking reaction times, computational results, degradation of separated NCNCs with hMPO/H_2O_2/NaCl, degradation of separated NCNCs with NaClO, separated NCNCs treated only with H_2O_2, degradation of GNP-corked NCNCs with NaClO, GNP-corked NCNCs treated with H_2O_2, GNP-corked NCNCs treated with hMPO and H_2O_2, TEM images of GNP-NCNCs from neutrophils without incubation, TEM images of GNP-NCNCs loaded with Rh123 and paclitaxel, Raman and fluorescence spectra of washed Rh123 loaded GNP-NCNCs, flow cytometry of NCNCs showing noncytotoxic behavior, and differentiation of MDSC to DC. This material is available free of charge via the Internet at http://pubs.acs.org.

■ AUTHOR INFORMATION

Corresponding Author

astar@pitt.edu

Notes

The authors declare no competing financial interest.

■ ACKNOWLEDGMENTS

This work at the University of Pittsburgh was supported by an NSF CAREER Award No. 0954345, NIH R01ES019304, RO1 CA154369, U19 AI068021, HL114453, and NIOSH OH008282. We thank the Nanoscale Fabrication and Characterization Facility and the Department of Biological Sciences at the University of Pittsburgh for provision of access to the TEM and Raman instruments and acknowledge R. J. Lee's group for access to the XPS instrumentation. Y.Z. is thankful for support from a Bayer Material Science Fellowship.

■ REFERENCES

(1) Matsumura, Y.; Maeda, H. *Cancer Res.* **1986**, *46*, 6387.
(2) Allen, T. M.; Cullis, P. R. *Science* **2004**, *303*, 1818.
(3) O'Neal, D. P.; Hirsch, L. R.; Halas, N. J.; Payne, J. D.; West, J. L. *Cancer Lett.* **2004**, *209*, 171.
(4) Maeda, H. *J. Controlled Release* **2012**, *164*, 138.
(5) Portney, N. G.; Ozkan, M. *Anal. Bioanal. Chem.* **2006**, *384*, 620.
(6) Emerich, D. F.; Thanos, C. G. *J. Drug Targeting* **2007**, *15*, 163.
(7) Torchilin, V. P. *Annu. Rev. Biomed. Eng.* **2006**, *8*, 343.
(8) Chen, J.; Chen, S.; Zhao, X.; Kuznetsova, L. V.; Wong, S. S.; Ojima, I. *J. Am. Chem. Soc.* **2008**, *130*, 16778.
(9) Wu, W.; Wieckowski, S.; Pastorin, G.; Benincasa, M.; Klumpp, C.; Briand, J. P.; Gennaro, R.; Prato, M.; Bianco, A. *Angew. Chem., Int. Ed.* **2005**, *44*, 6358.
(10) Prato, M.; Kostarelos, K.; Bianco, A. *Acc. Chem. Res.* **2007**, *41*, 60.
(11) Liu, Z.; Sun, X.; Nakayama-Ratchford, N.; Dai, H. *ACS Nano* **2007**, *1*, 50.
(12) Ren, Y.; Pastorin, G. *Adv. Mater.* **2008**, *20*, 2031.
(13) Kim, B. M.; Qian, S.; Bau, H. H. *Nano Lett.* **2005**, *5*, 873.
(14) Guven, A.; Rusakova, I. A.; Lewis, M. T.; Wilson, L. J. *Biomaterials* **2012**, *33*, 1455.
(15) Yanagi, K.; Miyata, Y.; Kataura, H. *Adv. Mater.* **2006**, *18*, 437.
(16) Shekunov, B. Y.; Chattopadhyay, P.; Tong, H. H.; Chow, A. H. *Pharm. Res.* **2007**, *24*, 203.
(17) Owens, D. E., III; Peppas, N. A. *Int. J. Pharm.* **2006**, *307*, 93.
(18) Allen, B. L.; Kichambare, P. D.; Star, A. *ACS Nano* **2008**, *2*, 1914.
(19) Allen, B. L.; Shade, C. M.; Yingling, A. M.; Petoud, S.; Star, A. *Adv. Mater.* **2009**, *21*, 4692.
(20) Zhao, Y.; Tang, Y.; Chen, Y.; Star, A. *ACS Nano* **2012**, *6*, 6912.
(21) Gong, K.; Du, F.; Xia, Z.; Durstock, M.; Dai, L. *Science* **2009**, *323*, 760.
(22) Tang, Y.; Allen, B. L.; Kauffman, D. R.; Star, A. *J. Am. Chem. Soc.* **2009**, *131*, 13200.
(23) Tang, Y.; Burkert, S. C.; Zhao, Y.; Saidi, W. A.; Star, A. *J. Phys. Chem. C* **2013**, *117*, 25213.
(24) Ma, X.; Wang, E.; Tilley, R.; Jefferson, D.; Zhou, W. *Appl. Phys. Lett.* **2000**, *77*, 4136.
(25) Kim, Y.; Hayashi, T.; Fukai, Y.; Endo, M.; Yanagisawa, T.; Dresselhaus, M. *Chem. Phys. Lett.* **2002**, *355*, 279.
(26) Shimamoto, D.; Fujisawa, K.; Muramatsu, H.; Hayashi, T.; Kim, Y. A.; Yanagisawa, T.; Endo, M.; Dresselhaus, M. S. *Carbon* **2010**, *48*, 3643.
(27) Tang, Y.; Zhao, Y.; Burkert, S. C.; Ding, M.; Ellis, J. E.; Star, A. *Carbon* **2014**, *80*, 583.
(28) Zhao, Y.; Tang, Y.; Star, A. *J. Visualized Exp.* **2013**, e50383.
(29) Lemarchand, C.; Gref, R.; Couvreur, P. *Eur. J. Pharm. Biopharm.* **2004**, *58*, 327.
(30) Kam, N. W. S.; Liu, Z.; Dai, H. *J. Am. Chem. Soc.* **2005**, *127*, 12492.
(31) Nakayama-Ratchford, N.; Bangsaruntip, S.; Sun, X.; Welsher, K.; Dai, H. *J. Am. Chem. Soc.* **2007**, *129*, 2448.
(32) Volodkin, D. V.; Skirtach, A. G.; Möhwald, H. *Angew. Chem., Int. Ed.* **2009**, *48*, 1807.
(33) Poland, C. A.; Duffin, R.; Kinloch, I.; Maynard, A.; Wallace, W. A.; Seaton, A.; Stone, V.; Brown, S.; MacNee, W.; Donaldson, K. *Nat. Nanotechnol.* **2008**, *3*, 423.
(34) Kotchey, G. P.; Zhao, Y.; Kagan, V. E.; Star, A. *Adv. Drug Delivery Rev.* **2013**, *65*, 1921.
(35) Carrero-Sanchez, J.; Elias, A.; Mancilla, R.; Arrellin, G.; Terrones, H.; Laclette, J.; Terrones, M. *Nano Lett.* **2006**, *6*, 1609.
(36) Zhao, M.; Li, D.; Yuan, L.; Yue, Y.; Liu, H.; Sun, X. *Carbon* **2011**, *49*, 3125.
(37) Allen, B. L.; Kichambare, P. D.; Gou, P.; Vlasova, I. I.; Kapralov, A. A.; Konduru, N.; Kagan, V. E.; Star, A. *Nano Lett.* **2008**, *8*, 3899.
(38) Allen, B. L.; Kotchey, G. P.; Chen, Y.; Yanamala, N. V.; Klein-Seetharaman, J.; Kagan, V. E.; Star, A. *J. Am. Chem. Soc.* **2009**, *131*, 17194.
(39) Kagan, V. E.; Konduru, N. V.; Feng, W.; Allen, B. L.; Conroy, J.; Volkov, Y.; Vlasova, I. I.; Belikova, N. A.; Yanamala, N.; Kapralov, A.; Tyurina, Y. Y.; Shi, J.; Kisin, E. R.; Murray, A. R.; Franks, J.; Stolz, D.; Gou, P.; Klein-Seetharaman, J.; Fadeel, B.; Star, A.; Shvedova, A. A. *Nat. Nanotechnol.* **2010**, *5*, 354.

DOI: 10.1021/ja511843w
J. Am. Chem. Soc. 2015, 137, 675−684

(40) Zhao, Y.; Allen, B. L.; Star, A. *J. Phys. Chem. A* **2011**, *115*, 9536.
(41) Russier, J.; Ménard-Moyon, C.; Venturelli, E.; Gravel, E.; Marcolongo, G.; Meneghetti, M.; Doris, E.; Bianco, A. *Nanoscale* **2011**, *3*, 893.
(42) Hampton, M. B.; Kettle, A. J.; Winterbourn, C. C. *Blood* **1998**, *92*, 3007.
(43) Boateng, J. S.; Matthews, K. H.; Stevens, H. N.; Eccleston, G. M. *J. Pharm. Sci.* **2008**, *97*, 2892.
(44) Rodriguez, P. C.; C, O. A. *Immunol. Rev.* **2008**, *222*, 180.
(45) Ko, J. S.; KBukowski, R. M.; Fincke, J. H. *Curr. Oncol. Rep.* **2009**, *11*, 87.
(46) Wang, E. G. *J. Mater. Res.* **2006**, *21*, 2767.
(47) Ding, M.; Sorescu, D. C.; Kotchey, G. P.; Star, A. *J. Am. Chem. Soc.* **2012**, *134*, 3472.
(48) Ding, M.; Tang, Y.; Star, A. *J. Phys. Chem. Lett.* **2013**, *4*, 147.
(49) Attal, S.; Thiruvengadathan, R.; Regev, O. *Anal. Chem.* **2006**, *78*, 8098.
(50) Fu, X.; Bei, F.; Wang, X.; O'Brien, S.; Lombardi, J. R. *Nanoscale* **2010**, *2*, 1461.
(51) Sylvestre, J.-P.; Poulin, S.; Kabashin, A. V.; Sacher, E.; Meunier, M.; Luong, J. H. *J. Phys. Chem. B* **2004**, *108*, 16864.
(52) Jansen, R. J. J.; van Bekkum, H. *Carbon* **1995**, *33*, 1021.
(53) Chiu, C. F.; Barth, B. A.; Kotchey, G. P.; Zhao, Y.; Gogick, K. A.; Saidi, W. A.; Petoud, S.; Star, A. *J. Am. Chem. Soc.* **2013**, *135*, 13356.
(54) Rout, C. S.; Kumar, A.; Xiong, G.; Irudayaraj, J.; Fisher, T. S. *Appl. Phys. Lett.* **2010**, *97*, 133108.
(55) Chowdhury, J.; Pal, P.; Ghosh, M.; Misra, T. *J. Colloid Interface Sci.* **2001**, *235*, 317.
(56) Ling, J.; Weitman, S. D.; Miller, M. A.; Moore, R. V.; Bovik, A. C. *Appl. Opt.* **2002**, *41*, 6006.
(57) Gabrilovich, D. I.; Nagaraj, S. *Nat. Rev. Immunol.* **2009**, *9*, 162.
(58) Shurin, G. V.; Ouellette, C. E.; Shurin, M. R. *Cancer Immunol. Immunother.* **2012**, *61*, 223.
(59) Mantovani, A.; Sica, A. *Curr. Opin. Immunol.* **2010**, *22*, 231.
(60) Younos, I.; Donkor, M.; Hoke, T.; Dafferner, A.; Samson, H.; Westphal, S.; Talmadge, J. *Int. Immunopharmacol.* **2011**, *11*, 816.
(61) Gregory, A. D.; Houghton, A. M. *Cancer Res.* **2011**, *71*, 2411.
(62) Zhong, H.; Dmitriy, G. W.; Han, B.; Ma, Y.; Keskinov, A. A.; Shurin, M. R.; Shurin, G. V. *Int. J. Cancer* **2014**, *134*, 2633.
(63) Michels, T.; Shurin, G. V.; Naiditch, H.; Sevko, A.; Umansky, V.; Shurin, M. R. *J. Immunotoxicol.* **2012**, *9*, 292.
(64) Shurin, G. V.; Tourkova, I. L.; Kaneno, R.; Shurin, M. R. *J. Immunol.* **2009**, *183*, 137.
(65) Shurin, G. V.; Tourkova, I. L.; Shurin, M. R. *J. Immunother.* **2008**, *31*, 491.
(66) Sevko, A.; Michels, T.; Vrohlings, M.; Umansky, L.; Beckhove, P.; Kato, M.; Shurin, G. V.; Shurin, M. R.; Umansky, V. *J. Immunol.* **2013**, *190*, 2464.

DOI: 10.1021/ja511843w
J. Am. Chem. Soc. 2015, 137, 675−684